

CPath-Omni: A Unified Multimodal Foundation Model for Patch and Whole Slide Image Analysis in Computational Pathology

^{1,2}Yuxuan Sun*, ¹Yixuan Si*, ¹Chenglu Zhu, ³Xuan Gong, ⁴Kai Zhang, ^{1,2}Pingyi Chen,
⁵Ye Zhang, ^{1,2}Zhongyi Shui, ¹Tao Lin†, ¹Lin Yang†

¹Westlake University, ²Zhejiang University, ³Harvard University,

⁴The Ohio State University, ⁵University of the Chinese Academy of Sciences

Abstract

The emergence of large multimodal models (LMMs) has brought significant advancements to pathology. Previous research has primarily focused on separately training patch-level and whole-slide image (WSI)-level models, limiting the integration of learned knowledge across patches and WSIs, and resulting in redundant models. In this work, we introduce CPath-Omni, the first 15-billion-parameter LMM designed to unify both patch and WSI level image analysis, consolidating a variety of tasks at both levels, including classification, visual question answering, captioning, and visual referring prompting. Extensive experiments demonstrate that CPath-Omni achieves state-of-the-art (SOTA) performance across seven diverse tasks on 39 out of 42 datasets, outperforming or matching task-specific models trained for individual tasks. Additionally, we develop a specialized pathology CLIP-based visual processor for CPath-Omni, CPath-CLIP, which, for the first time, integrates different vision models and incorporates a large language model as a text encoder to build a more powerful CLIP model, which achieves SOTA performance on nine zero-shot and four few-shot datasets. Our findings highlight CPath-Omni’s ability to unify diverse pathology tasks, demonstrating its potential to streamline and advance the field of foundation model in pathology.

1. Introduction

Pathology plays a pivotal role in modern medicine, serving as the foundation for diagnosing and understanding diseases [28]. However, pathology requires significant human effort to conduct precise and accurate interpretations of images that can be as large as $100,000 \times 100,000$ pixels.

In recent years, with advancements in computational power and the digitization of pathology, a wide range of

*Equal contribution.

†Corresponding author.

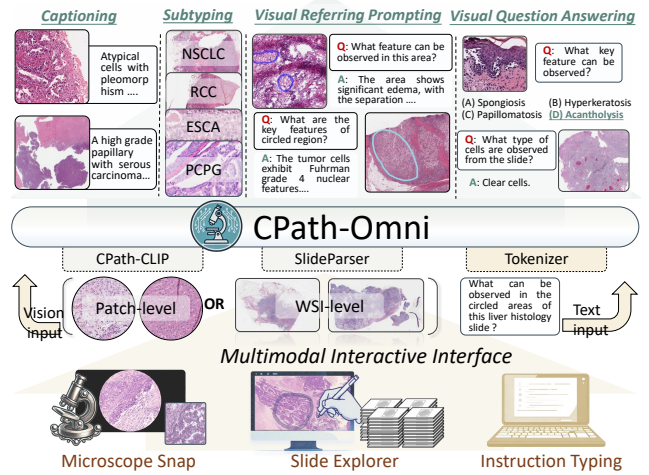


Figure 1. Overview of CPath-Omni’s ability to handle both patch-level and WSI analysis in clinical environments, such as microscope views and scanned WSIs, while supporting various tasks.

models have been developed to assist pathologists in their diagnostic tasks. These include CLIP [38]-based patch processing models like CONCH [32] and PathGen-CLIP [46], DINOv2 [36]-based models like Virchow2 [61] and UNI [11], and LMMs like PathAsst [47], PathGen-LLaVA [46], Quilt-LLaVA [41], and PathChat [33], which support tasks such as multi-turn conversations. At the WSI level, models like Prov-GigaPath [56] and HIPT [10] are developed for WSI classification, while models such as HistGen [14] and WsiCaption [8] are used to generate WSI reports.

In this work, we propose CPath-Omni, a multimodal foundation model designed to unify patch-level and WSI-level analysis. CPath-Omni can perform diverse tasks such as VQA, classification, captioning, and visual referring prompting. By integrating these two levels of analysis and enabling generalizable task performance, CPath-Omni represents a significant step toward developing a truly versatile and comprehensive assistive tool for pathologists.

We first train a novel pathology-specific foundation model, CPath-CLIP, to serve as the vision encoder for CPath-Omni. CPath-CLIP is the first model to integrate a large language model (LLM) as the text encoder for CLIP, while also incorporating the self-supervised pathology vision model Virchow2 as the visual encoder, alongside the original CLIP-L model. To train CPath-CLIP, we collect 700,145 image-caption pairs from diverse datasets, constructing CPath-PatchCaption. Then, we integrate CPath-CLIP into the large language model Qwen2.5-14B [17] to equip it with visual capabilities, creating the CPath-Omni.

The training of CPath-Omni proceeds through four stages to build a unified model capable of handling both patch-level and WSI-level tasks. In the first stage, we pre-align CPath-CLIP with the Qwen2.5-14B language model using the CPath-PatchCaption dataset. Next, we collect and construct 351,871 instruction tuning samples from four diverse patch-level tasks across 21 datasets, including patch-level classification, VQA, captioning, and visual referring prompting. In stage 3, we introduce WSI-related data, including 5,850 cleaned WSI reports, to continue pretraining CPath-Omni, further enhancing its WSI understanding based on the previous stage. In the final stage, we construct 33,830 WSI instruction tuning samples from three tasks across nine datasets, including classification, VQA, and captioning, along with 15% patch-level instruction tuning samples for joint WSI-Patch training. This joint training enables CPath-Omni to seamlessly process both patch and WSI data and enables a wide range of downstream tasks.

Extensive experiments across seven diverse tasks and 42 datasets are conducted to validate the effectiveness of CPath-Omni. With its broad capabilities, CPath-Omni achieves state-of-the-art (SOTA) performance on 39 out of 42 datasets and demonstrates comparable or superior performance to task-specific models. The main contributions of our study are summarized as follows:

- We develop **CPath-CLIP**, the most powerful pathology CLIP model to date, which achieves SOTA results on 9 zero-shot and 4 linear probing classification datasets.
- We introduce **CPath-Omni**, the first unified model capable of handling both patch-level and WSI analysis across diverse tasks, offering exceptional performance and versatility, and representing an early realization of the “one-for-all” paradigm in computational pathology.
- We curate a diverse and comprehensive training and testing dataset, spanning 7 tasks across 42 datasets, making it the largest and most diverse dataset for training LMMs in pathology. Extensive experiments are conducted on these datasets to confirm CPath-Omni’s significant advancement in pathology foundation models.

2. Related Work

Vision Foundation Models in Pathology. In recent years, with the rapid advancement of digital pathology slide digitization, pathology-specific visual foundation models (VFMs) have made significant strides. These models are primarily divided into two main categories. The first is the Vision-Language-based model, such as CLIP [38], which employs contrastive learning to align images with textual descriptions, enabling the vision encoder to generate semantically meaningful features. Researchers have compiled large datasets of image-caption pairs from sources such as PubMed, YouTube, Twitter, and books to train these models. Notable examples in this category include Quilt-Net [19], PLIP [16], PathCLIP [47], PathGen-CLIP [46], and CONCH [32]. The second category focuses on vision-only models, trained through self-supervised learning using vast amounts of patch data extracted from WSIs. These models are typically trained with techniques like DINO [7, 36] pre-training to learn robust visual representations. Prominent models in this group include Lunit [24], UNI [11], ProV-GigaPath [56], and Virchow series [51, 61].

The development of pathology-specific VFMs has significantly improved image representations, enhancing performance on downstream tasks like patch and WSI classification. CLIP-based models, which are pre-aligned with textual information, are easier to integrate with LLMs. In contrast, DINO-based models tend to learn more fine-grained visual features [23]. In this paper, we combine the strengths of both approaches by leveraging OpenAI-CLIP-L and the vision-only Virchow2 as our visual encoder, aligned with the Qwen2-1.5B [57] LLM to enhance visual capabilities and improve alignment with LLM world knowledge.

Multimodal Generative Foundation Models in Pathology. The integration of LLMs like GPT-4 [34] with vision capabilities has led to advanced LMMs such as GPT-4V [35] and Gemini Pro Vision [48]. These LMMs offer generalized capabilities, which are particularly well-suited to the field of pathology, where understanding a broad range of diseases (e.g., lung cancer, liver cancer), adapting to various tissues (e.g., prostate, colon, stomach), and performing across diverse tasks (e.g., tumor classification, survival prediction) is essential. As a result, numerous pathology-specific LMMs have been developed, building on these general LLMs and LMMs. Notable models include PathAsst [47], PathGen-LLaVA [46], Quilt-LLaVA [40], and PathChat [33], which demonstrate strong image understanding and multi-turn conversational abilities. However, due to input size constraints, these models primarily focus on patch-level tasks.

Recently, several works have trained smaller multimodal language models for WSI tasks. For example, WsiCaption [8] and HistGen [14] focus on WSI caption generation, while WSI-VQA [9] targets WSI-based VQA. The former

primarily uses publicly available datasets with fewer than 10,000 samples. More recently, The PRISM [42], trained on 587,196 internal WSIs, developed a CoCa [58]-like model capable of zero-shot WSI classification and WSI report generation, representing a significant step toward to more generalizable generative foundation models.

Multimodal Datasets in Pathology. To construct powerful CLIP-based models, a large volume of high-quality image-caption pairs is essential. In the patch-level domain, the ARCH [13] dataset collects 8,617 figure-caption pairs related to histology images from medical articles and textbooks. The PathCap [47] dataset contains 207,000 pathology image-caption pairs, carefully curated from over 15 million image-text pairs sourced from PubMed and various textbooks. The OpenPath [16] dataset includes 208,414 pairs collected from Twitter posts, while the QUILT-1M [19] dataset contains 768,826 histopathology image-text pairs derived from YouTube video frames. Additionally, to train LMMs, Quilt-Instruct [40] generated 107,131 instruction-tuning samples from YouTube lectures, while PathGen-Instruct [46] created 200K instruction-tuning samples based on synthetic captions from the PathGen-1.6M.

In the WSI domain, the available data is much more limited. WsiCaption [8] and HistGen [14] generate 10,000 and 7,753 WSI captioning samples based on TCGA report PDFs, respectively. More recently, WSI-VQA [9] expanded these WSI report datasets to create the WSI VQA dataset.

In this paper, we systematically compile these existing datasets and augment them with additional processing. We also incorporate our downstream datasets as the foundation for the training and testing of CPath-Omni.

3. Data Preparation

In this section, we introduce the patch-level and WSI-level data required for constructing CPath-Omni.

3.1. Patch Level Dataset

CPath-PatchCaption: This dataset is a curated image-caption pairs dataset consisting of 700,145 pairs gathered from various open-source datasets. Specifically, it includes 218,630 pairs from PathCap, 388,932 pairs from Quilt-1M, and 92,583 pairs from OpenPath. We ensured that this caption dataset does not overlap with the test data used in Path-Omni. This dataset serves as a key component for pretraining CPath-CLIP and the stage 1 pretraining of CPath-Omni.

CPath-PatchInstruction: CPath-PatchInstruction is a diverse dataset consisting of 351,871 samples across captioning, VQA, classification, and visual referring prompting tasks. Of these, 147,843 examples are sourced from CPath-PatchCaption, representing the highest-quality samples curated by human annotators. Captions and images were further refined using GPT-4 to generate more

detailed captions, enhancing CPath-Omni’s powerful image understanding capabilities. Additionally, 40,000 examples were drawn from PathInstruct, a multimodal, multi-turn conversational dataset. For the classification data, samples were collected from various public classification datasets, including VALSET-TCGA, VALSET-WNS, VALSET-CHA [49], Stomach, KIRC, CocaHis [45], PAIP23, BNCB [54], CATCH [53], PAIP21, MIDOG22 [4], KICH, CAMEL [55], Gleason-CNN [3], OCELOT [39], and NASNetLarge [62]. No more than 5,000 data points were randomly sampled from each dataset, with 80% converted into VQA format for CPath-Instruction training and 20% reserved for validation and testing. To further enhance the model’s capabilities and interpretability, we collaborate with expert pathologists who annotate 1,300 high-resolution images randomly selected from TCGA. The annotations are initially processed by GPT-4 to generate preliminary findings of the images, which are then meticulously revised, supplemented, and refined by pathologists for accuracy. Most importantly, corresponding areas for each pathology finding are highlighted in the images to create visual referring prompting data. Of these, 1,200 data points are used for training, and 100 are designated for validation and testing. The entire CPath-PathInstruction dataset is used for stage 2 training of CPath-Omni. For further construction and annotation details, please refer to the Appendix.

3.2. WSI Level Dataset

CPath-WSIInstruction: CPath-WSIInstruction encompasses captioning, VQA, and classification data at the WSI level. The dataset includes 7,312 WSI-level captioning examples sourced from HistGen. To ensure that the validation and test sets do not overlap with the WSI classification data, we re-divide the data into training, validation, and test sets with an 8:1:1 ratio. The training set is incorporated into CPath-WSIInstruction. For the VQA component, we further generate a WSI VQA dataset by prompting GPT-4 based on the divided WSI captions. Specific prompts are detailed in the Appendix. For classification, we compile subtype data for 8 TCGA subtyping tasks, including RCC, NSCLC, BRCA, UCEC, THCA, ESCA, BLCA, and TGCT. 80% of this data is transformed into the QA format that CPath-Omni can accept for training, while the remaining 10% is reserved for validation and testing.

4. The Proposed CPath-Omni

As shown in Fig. 1, CPath-Omni’s architecture consists of two vision components, CPath-CLIP (for patch-level image processing) and SlideParser (for WSI-level image processing), along with an LLM. Patch and WSI inputs are processed through their respective branches. These vision modules encode patch-level or WSI-level visual tokens, which are then fed as input to the LLM. For the LLM,

we choose the latest Qwen2.5 14B model as part of CPath-Omni. In this section, we provide a detailed description of the construction of CPath-CLIP and SlideParser.

4.1. CPath-CLIP

Pretrained CLIP models are commonly used with LLMs in general-domain LMMs, as they are well-aligned with the text space and are easier to integrate with LMMs. However, pathology images differ significantly from natural images, creating a domain gap that limits CLIP performance in pathology tasks. Therefore, a pathology-specific CLIP-based model should be constructed to improve image understanding and enhance LMM performance in this domain.

One challenge with CLIP models is their focus on coarse-grained semantic information, which can cause the loss of fine-grained details critical for pathology diagnoses, such as chromatin structure or mitosis. To address this, we integrate the pretrained Virchow2 model, trained on 3 million WSIs using DINOv2-based vision pretraining, providing strong visual representations. We also retain OpenAI’s CLIP vision component to preserve robust semantic features. As shown in the left part of Fig. 2, we feed the image into both models and concatenate their feature outputs. To further improve the alignment between the vision model and the LLM, we replace the GPT-2 model used in the original CLIP architecture with Qwen2-1.5B, a model from the same framework as the LLM. Due to its larger size and broader training corpus, Qwen2-1.5B brings stronger world knowledge, significantly improving the semantic alignment between the vision and language components. Specifically, we train CPath-CLIP using the CPath-PathCaption dataset based on OpenCLIP framework [21].

When used for patch processing in CPath-Omni, CPath-CLIP adopts the AnyRes strategy from Llava-Next [31] to handle higher resolutions. Each image is split into a 3×3 grid of sub-patches, which are encoded by CPath-CLIP to extract features. These features are then processed through a two-layer MLP before being input into the LLM.

4.2. SlideParser

SlideParser is the core component for handling WSI inputs, particularly for gigapixel images up to $100,000 \times 100,000$ pixels. To manage this, we first split the WSI into multiple 2048×2048 image regions. As pathologists often require both global and local context during analysis, we incorporate a multi-scale region encoding approach. As shown in Fig. 2. Each 2048×2048 region is further subdivided into three scales: 16 tiles of 512×512 , 4 tiles of 1024×1024 , and 1 tile of 2048×2048 . These tiles are then encoded by CPath-CLIP to generate image-level features, which are aggregated using average pooling to produce a final multi-scale feature representation for the 2048×2048 region, which also significantly reduces the number of image to-

kens input into the LLM.

Since WSIs can vary greatly in size—from dozens to thousands of patches—this variability can cause instability during LMM training. To address this, we introduce a token compression layer that standardizes the input by reducing WSI tokens to a fixed length. Specifically, we adopt the CoCa approach [58], using 1152 query tokens through multi-head attention to query the patch tokens, resulting in a unified output of 1152 tokens for the LLM.

4.3. The Training of CPath-Omni

The construction of CPath-Omni undergoes four training stages: patch-based pretraining, finetuning, WSI-based pretraining, and mixed patch-WSI training.

Stage 1: In this stage, we focus on aligning the feature spaces of CPath-CLIP and the LLM. Only the two-layer MLP connecting CPath-CLIP to the LLM is trained, using the CPath-PatchCaption dataset. This enables the model to pre-align visual and language features.

Stage 2: We unfreeze all model parameters and finetune using the CPath-PatchInstruct dataset. Building on the alignment from Stage 1, this stage enables CPath-Omni to learn a variety of tasks, including VQA, image classification, captioning, and pathology-related knowledge.

Stage 3: In this stage, training uses WSI report-only data. Only SlideParser is unfrozen to align WSI features with the pathology-related knowledge already learned by the LLM from patch-based training.

Stage 4: The final stage introduces mixed training with 15% randomly sampled CPath-PathInstruct and CPath-WSIInstruct datasets. By this point, CPath-Omni has gained a strong understanding of pathology from previous stages, enabling effective transfer of patch-based knowledge to WSI tasks, despite the limited WSI data.

After completing these four stages, CPath-Omni is fully equipped to effectively handle both patch-based and WSI analysis across a variety of downstream tasks.

5. Experiments

We conducted extensive experiments to evaluate the universal task-solving capabilities of CPath-Omni. At the patch level, we evaluated across 32 subsets, covering tasks such as VQA, classification, captioning, and visual referring prompting (VPR). For the WSI level, we evaluated 10 subsets focusing on WSI VQA, classification, and captioning.

5.1. Benchmarking CPath-CLIP

In our experiments, we evaluated the image-text alignment and feature extraction capabilities of CPath-CLIP through zero-shot classification and few-shot linear probing. For zero-shot classification, we utilized datasets including PatchCamelyon (Pcam) [50], CRC-100K [25],

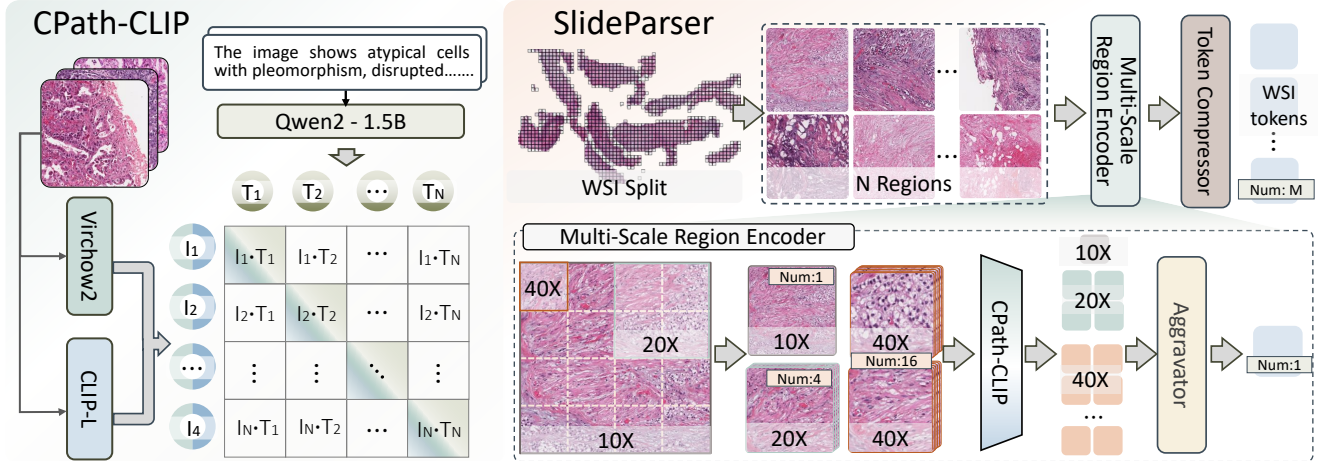


Figure 2. Overview of two key vision components of CPath-Omni: the patch-level model, CPath-CLIP, and the WSI model, SlideParser.

Model	LC-Lung	LC-Colon	CRC100K	SkinCancer	Pcam	BACH	Osteo	WSSSLUAD	SICAPv2	Average
OpenAI-CLIP-L	70.4	81.1	40.3	19.4	55.5	34.3	53.9	81.2	25.4	51.3
PLIP	87.9	90.2	52.8	42.5	51.8	34.3	52.9	73.1	42.5	58.6
QuiltNet	80.0	91.0	49.5	46.4	58.7	43.8	53.8	70.5	37.3	58.9
PathCLIP	88.9	94.3	55.3	35.1	72.5	46.8	69.2	<u>85.1</u>	48.3	66.2
BiomedCLIP	48.8	94.3	29.9	31.7	84.0	39.8	36.7	73.7	32.2	52.9
PathGen-CLIP-L	89.8	<u>99.3</u>	78.0	<u>70.6</u>	<u>88.2</u>	<u>71.5</u>	<u>74.6</u>	82.2	63.5	<u>79.7</u>
CPath-CLIP	97.1	100.0	78.0	74.2	95.9	72.3	80.7	87.1	<u>63.1</u>	83.2

Table 1. Zero-shot classification comparison of various CLIP models on different pathology image classification datasets with accuracy (%). The best performance is highlighted in **bold**, while the second-best is underlined.

SICAPv2 [43], BACH [1], Osteo [2], SkinCancer [27], WSSSLUAD [15], LC-Lung, and LC-Colon [6]. Our model’s performance was benchmarked against OpenAI-CLIP-L [37], PLIP [16], QuiltNet [20], PathCLIP [47], BiomedCLIP [60], and the SOTA PathGen-CLIP-L [46].

Results: CPath-CLIP achieved superior performance across most datasets. As shown in Tab. 1, CPath-CLIP notably surpasses the current SOTA model, PathGen-CLIP-L by a significant margin on the Osteo, Pcam, and LC-Lung datasets, with improvements of 6.1%, 7.7% and 7.3%, respectively. Additionally, it demonstrated significant advantages over other models, underscoring CPath-CLIP’s enhanced image-text feature alignment capabilities driven by its stronger vision and language model integration.

For few-shot linear probing, we added a fully connected layer to extracted feature representations from four datasets: LC-Colon, Camelyon17, LC-Lung, and WSSSLUAD, using training sizes of 2, 8, 16, 32, 64, and 128 shots. Each size was randomly sampled 10 times and evaluated over 10 runs per configuration. Box plots are utilized to illustrate the variability and robustness of the model’s performance.

Results: CPath-CLIP consistently outperformed previous models. As shown in Fig. 3, CPath-CLIP demonstrated rapid improvement with minimal data, reaching 95% accu-

racy on CRC and LC-Lung using only 2 shots. In contrast, other models achieved less than 91% accuracy on CRC and approximately 92% on LC-Lung.

We hypothesize that using advanced LLMs as CLIP’s text encoder provides superior world knowledge compared to previous approaches using BERT or GPT-2. When combined with pathology-specific vision model Virchow2, this integration can achieve faster and more effective alignment. Unlike general CLIP-based models that require 400 million to billions of training samples, CPath-CLIP was trained with only 700K samples, which holding great potential to redefine future CLIP training paradigms.

5.2. Benchmarking CPath-Omni at Patch-Level

At the patch level, we benchmark CPath-Omni against SOTA models, both general-purpose and domain-specific.

We begin by evaluating the performance of various LLMs on VQA using the PathMMU dataset, the largest pathology-specific VQA dataset, which also includes pathologist scores. We compare general-purpose models such as InstructBLIP-FLAN-T5 XXL [12], LLaVA-1.5-13B [30], Qwen-VL-MAX [5], Gemini Pro Vision [48], and GPT-4V [35], alongside domain-specific models such as LLaVA-Med, Quilt-LLaVA, and PathGen-LLaVA.

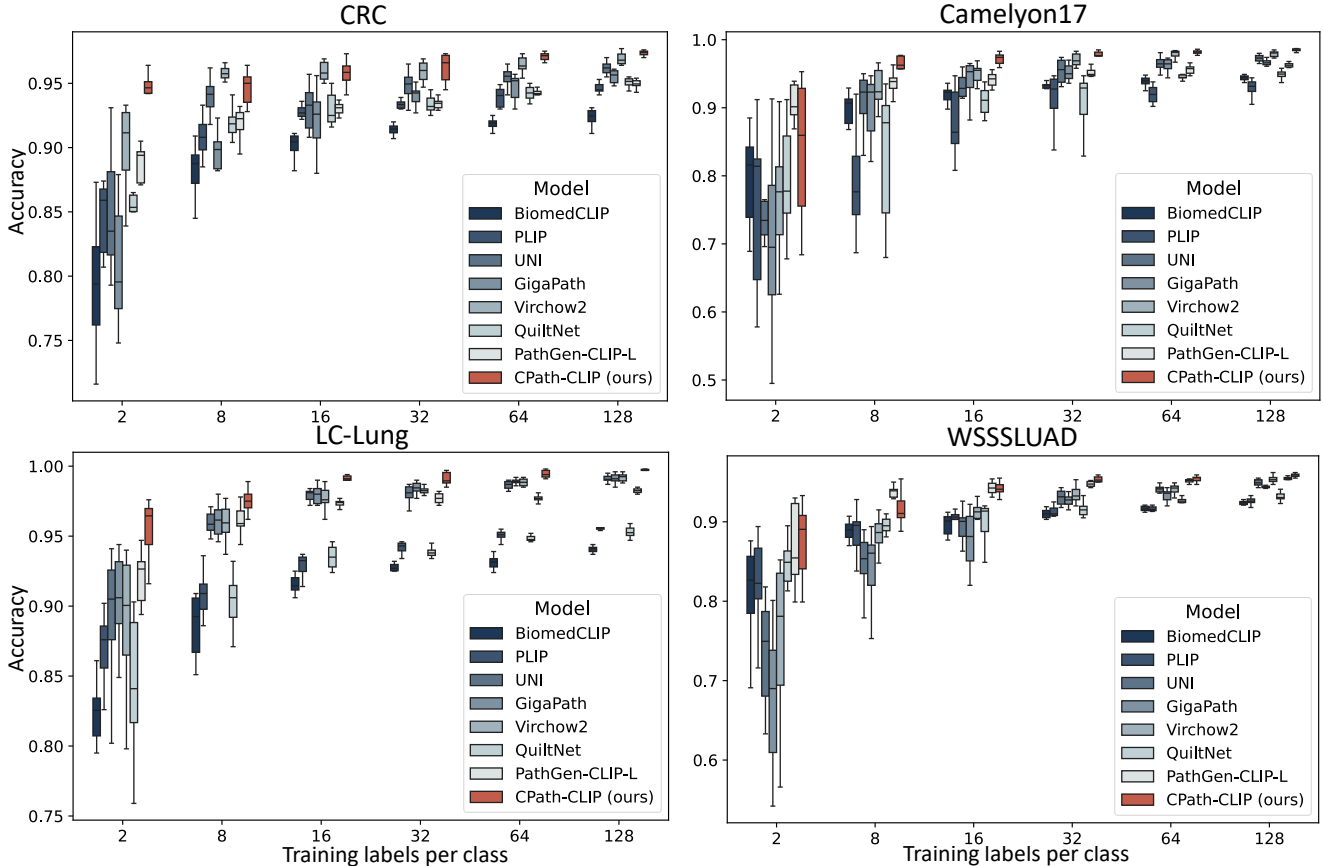


Figure 3. Comparison of few-shot classification accuracy (%) via linear probing across various datasets using different CLIP models.

Results: CPath-Omni significantly outperforms both the latest pathology-specific model, PathGen-LLaVA, and advanced general-purpose models, even surpassing human-level performance. As shown in Tab. 2, CPath-Omni exceeds the current SOTA model, PathGen-LLaVA, by 13.8%, with a particularly notable 30.1% improvement in PathCLS [59] performance. Moreover, it slightly surpasses the 71.8% accuracy achieved by human pathologists, by 0.6%. We attribute this to the fact that pathologists annotating the PathMMU dataset may not be experts in all disease categories, whereas foundation models like CPath- can learn generalized knowledge across diverse medical fields. This highlights that CPath-Omni has the promising potential of LMMs to offer valuable assistance to clinicians in real-world settings.

For the classification task, we evaluate performance across 30 classification datasets, including 16 in-distribution (ID) datasets—where the training data is part of CPath-Omni’s training set—such as VALSET-TCGA, VALSET-CHA, VALSET-WNS [49], Stomach, KIRC, CocaHis [45], PAIP23, BNCB [54], CATCH [53], PAIP21, MIDOG22 [4], KICH, CAMEL [55], Gleason-CNN [3], OCELOT [39], and NASNetLarge [62].

Additionally, we use 14 out-of-distribution (OOD) datasets that were not included in CPath-Omni’s training data, such as AGGC2022 [18], KIRP, PAIP19 [26], VALSET-TUKK, as well as 10 datasets from PathCLS within the PathMMU dataset, namely: Skincancer, LC25000-Lung, LC25000-Colon, CRC-100K [25], BACH, WSSSLUD, PatchCamlyon17, Osteo, MHIST [52], and SICAPv2 [44]. For all 30 datasets, we compare CPath-Omni with the state-of-the-art models GPT-4V and Gemini-1.5-Pro on their respective test sets. For the ID datasets, we also perform task-specific training with Virchow2, the previous SOTA vision-only model, to facilitate direct comparisons with CPath-Omni.

Results: CPath-Omni significantly outperforms both GPT-4V and Gemini-1.5-Pro, and even achieves performance comparable to a task-specific fine-tuned version of Virchow2 on each individual dataset. As shown in Fig. 4, the radar chart for CPath-Omni closely mirrors that of Virchow2, with performance varying across datasets. However, CPath-Omni holds a slight advantage in average performance. In contrast, for general-purpose models, CPath-Omni consistently outperforms GPT-4V, even on OOD datasets, demonstrating its superior capability and gener-

	Test Overall		PubMed		SocialPath		EduContent		Atlas		PathCLS	
	Tiny (1156)	ALL (9677)	Tiny (281)	ALL (3068)	Tiny (235)	All (1855)	Tiny (255)	All (1938)	Tiny (208)	ALL (1007)	Tiny (177)	ALL (1809)
Expert performance	71.8	-	72.9	-	71.5	-	69.0	-	68.3	-	78.9	-
General Large Multimodal Models												
InstructBLIP-FLAN-T5-XXL	34.3	33.9	39.1	37.2	33.6	34.3	34.5	36.0	38.5	39.3	22.6	22.7
LLaVA-1.5-13B	38.8	37.6	44.5	41.0	40.4	40.4	34.1	39.4	47.1	44.3	24.9	23.5
Qwen-VL-MAX	49.2	45.9	53.0	50.9	53.6	49.3	52.2	47.9	<u>51.4</u>	49.8	30.5	29.6
Gemini Pro Vision	42.8	42.7	43.8	44.9	42.4	42.0	43.5	43.7	49.5	49.4	32.8	<u>34.7</u>
GPT-4V-1106	<u>53.9</u>	<u>49.8</u>	<u>59.4</u>	<u>53.5</u>	<u>58.7</u>	<u>53.9</u>	<u>60.4</u>	<u>53.6</u>	48.1	<u>52.8</u>	<u>36.2</u>	33.8
Pathology-specific Large Multimodal Models												
LLaVA-Med	25.3	26.2	28.5	27.7	28.9	27.3	22.7	27.2	22.6	30.7	22.6	20.3
Quilt-LLaVA	45.6	41.5	47.3	42.6	46.4	46.6	51.8	45.3	46.2	42.7	32.2	29.2
PathGen-LLaVA	60.1	58.4	60.1	60.1	60.9	58.8	60.8	60.7	63.5	64.9	54.2	48.9
CPath-Omni	72.4	72.2	74.0	69.9	76.6	71.8	69.8	70.6	65.9	70.6	75.7	79.0

Table 2. Overall results of models on the PathMMU **test set**. The best-performing LMM in each subset for general and pathology domain LMMs is **in-bold**, and the top-performing LMM is underlined.

alization compared to the strongest general-purpose models. Interestingly, when examining the datasets from the PathCLS branch, CPath-Omni’s overall OOD performance is strikingly close to that of CLIP-based models in a zero-shot setting (refer to Tab. 1). This suggests that CPath-Omni effectively harnesses the power of vision models within its multimodal framework, achieving zero-shot visual classification performance comparable to that of CLIP.

For visual referring prompting and patch captioning, we compare CPath-Omni with domain-specific models such as PathGen-LLaVA, Quilt-LLaVA, and LLaVA-Med. We introduced a set of 50 manually annotated images and conducted both GPT-4V evaluation (by comparing model outputs to ground truth annotations from pathologists) and human evaluation.

Results: CPath-Omni significantly outperforms the comparison models in both GPT-4V and human evaluations, with the lowest win rate reaching 84% in the VPR task when compared to Quilt-LLaVA. Interestingly, CPath-Omni achieves an even higher win rate against PathGen-LLaVA in the VPR task, despite PathGen-LLaVA being a stronger overall model. We hypothesize that this performance difference arises from the differences in training data: Quilt-LLaVA is trained on videos from YouTube instructors, which may include scenarios resembling visual referring prompting, whereas PathGen-LLaVA is primarily trained on synthetic TCGA data, which lacks such data.

5.3. Benchmarking CPath-Omni at WSI-Level

In WSI tasks, we benchmark CPath-Omni against both general-purpose models and task-specific fine-tuned models of 3 WSI tasks across 10 datasets.

For the classification task, we evaluate eight TCGA

CPath-Omni VS.	GPT-4o-eval		Human-eval	
	VPR	Captioning	VPR	Captioning
PathGen-LLaVA	96%	82%	98%	80%
Quilt-LLaVA	84%	96%	90%	92%
LLaVA-Med	96%	98%	100%	100%

Table 3. Comparison of CPath-Omni performance on Patch-level VPR and Captioning tasks with GPT-4o-eval and Human-eval across different models. The number represent the percentage of CPath-Omni’s responses considered superior.

subtyping datasets, including RCC (Kidney Chromophobe, Kidney Renal Clear Cell Carcinoma, Kidney Renal Papillary Cell Carcinoma), NSCLC (Lung Adenocarcinoma, Lung Squamous Cell Carcinoma), BRCA (Invasive Ductal Carcinoma, Invasive Lobular Carcinoma), UCEC (Cystic Mucinous and Serous Neoplasms, Adenomas and Adenocarcinomas), THCA (Papillary Adenocarcinoma, Papillary Carcinoma Columnar Cell, Papillary Carcinoma Follicular Variant), ESCA (Adenomas and Adenocarcinomas, Squamous Cell Neoplasms), BLCA (Transitional Cell Carcinoma, Papillary Transitional Cell Carcinoma), and TGCT (Non-seminoma, Mixed-seminoma, Seminoma). For more detailed information, please refer to the Appendix.

Given that these subtyping tasks are incorporated in CPath-Omni’s training, we test on the held-out test set and compare CPath-Omni’s performance against task-specific models, including ABMIL [22], DSMIL [29], a pathology CoCa-style pre-trained model (PRISM), and GPT-4o.

For ABMIL and DSMIL, we use features extracted from WSI patches via CPath-CLIP as input and train the models for 20 epochs, selecting the best checkpoints from the evaluation set for testing on the test set. In PRISM, we use

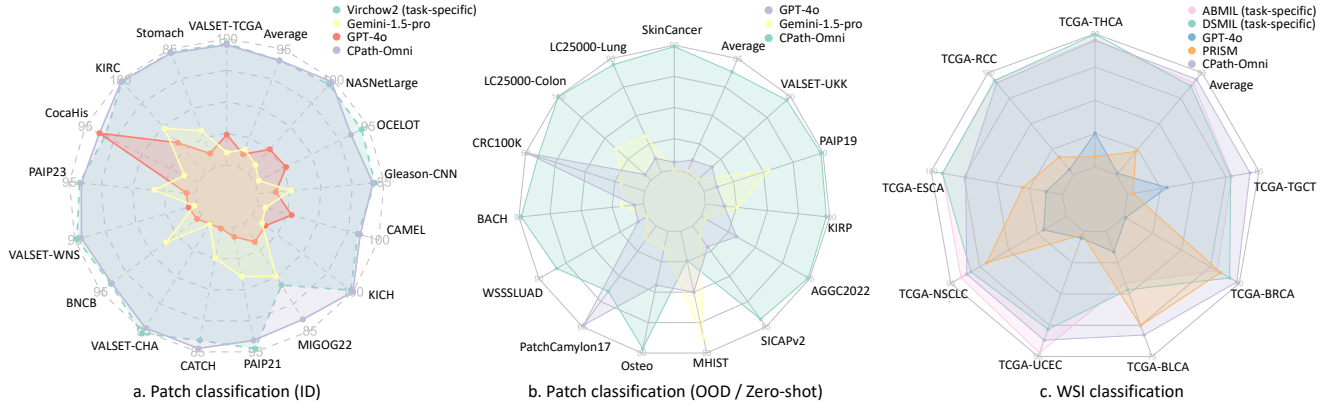


Figure 4. Radar plot visualization of CPath-Omni’s performance on patch and WSI classification tasks: (a) patch-level performance under ID conditions, (b) patch classification performance under OOD/zero-shot conditions, and (c) whole-slide image (WSI) performance.

the prompts from the PRISM paper for the eight subtyping tasks it covers. For tasks not included in PRISM, we use the TCGA subtyping classification names as prompts. For GPT-4V, since it does not directly support WSI diagnosis, we first split the WSI into 4096×4096 patches at 20X magnification. GPT-4V then generates descriptions for each patch, and these are merged to form a report for the entire slide. This report is subsequently used as input to prompt GPT-4V for classification of the WSI.

Results: *CPath-Omni significantly outperforms the general-purpose model GPT-4V and the pathology-specific foundation model PRISM, and demonstrates comparable or even superior performance to task-specific fine-tuned models such as ABMIL and DSMIL.* As shown in Fig. 4, CPath-Omni surpasses ABMIL and DSMIL on three tasks—TCGA-BLCA, TCGA-BRCA, and TCGA-TGCT—and shows a slight overall performance advantage over these models. This suggests that, in the future, a unified framework for WSI classification could achieve the performance of specialized models without the need for task-specific fine-tuning.

For WSI report generation, we compare CPath-Omni with task-specific models, including WsiCaption and HistGen, as well as the general-purpose model PRISM (also supports report generation) and GPT-4o (using the aforementioned method to generate WSI reports). Performance is evaluated using BLEU 1-4 and ROUGE-L scores. For VQA, since the first three models do not support it, we focus the comparison on CPath-Omni and GPT-4o, using the WSI reports generated by GPT-4o as context for answering questions. For closed-ended questions, accuracy is computed, while for open-ended questions, due to the brevity of answers, even small variations or synonyms can cause significant fluctuations in metrics like BLEU and recall. Therefore, we prompt GPT-4o to reference standard answers due to potential variations in BLEU and recall. Note that WSI

report generation and VQA tasks do not overlap with data used for WSI classification training.

Results: *CPath-Omni achieves SOTA performance in both WSI report generation and WSI VQA tasks, as shown in Tab. 4.* CPath-Omni slightly outperforms the previous SOTA model, HistGen. Note that PRISM tends to generate very short reports (often only a few words expressing the classification), which results in relatively lower performance metrics. In the WSI VQA task, CPath-Omni significantly outperforms GPT-4V, with performance metrics almost doubling: 67.3% vs. 20.5% for open-ended questions and 70.8% vs. 35.5% for closed-ended questions.

Model	Report Generation					VQA	
	BLEU ₁	BLEU ₂	BLEU ₃	BLEU ₄	ROUGE _L	Open	Closed
WsiCaption	21.8	13.7	8.6	6.4	25.1	-	-
HistGen	31.8	19.7	12.7	8.4	25.4	-	-
PRISM	0.0	0.0	0.0	0.0	8.0	-	-
GPT-4o	15.8	6.2	2.4	0.1	12.8	20.5	35.5
CPath-Omni	33.7	20.1	12.9	8.7	25.6	67.3	70.8

Table 4. Comparison of CPath-Omni’s performance with task-specific and general models on WSI captioning and VQA tasks.

6. Conclusion

In this paper, we present CPath-Omni, a versatile foundational multimodal model designed to tackle both patch-level and WSI-level tasks, spanning captioning, classification, VQA, and visual referring prompting. CPath-Omni’s approach enables unified patch and WSI-level training across 30 diverse datasets, allowing knowledge learned from the patch level to simultaneously enhance WSI performance, even trained on a fraction of the data compared to patch-level datasets. Extensive experiments demonstrate that CPath-Omni achieves superior performance across both patch and WSI-level tasks, comparable to or even outperforming task-specific models and significantly sur-

passing pretrained general-purpose foundation models like PRISM and GPT-4o. These results highlight the potential of LMMs like CPath-Omni to serve as a “one-for-all” solution, advancing the next generation of pathology-specific LMMs.

References

- [1] Guilherme Aresta, Teresa Araújo, Scotty Kwok, Sai Saketh Chennamsetty, Mohammed Safwan, Varghese Alex, Bahram Marami, Marcel Prastawa, Monica Chan, Michael Donovan, et al. Bach: Grand challenge on breast cancer histology images. *Medical image analysis*, 56:122–139, 2019. [5](#)
- [2] Harish Babu Arunachalam, Rashika Mishra, Ovidiu Daescu, Kevin Cederberg, Dinesh Rakheja, Anita Sengupta, David Leonard, Rami Hallac, and Patrick Leavey. Viable and necrotic tumor assessment from whole slide images of osteosarcoma using machine-learning and deep-learning models. *PLoS one*, 14(4):e0210706, 2019. [5](#)
- [3] Eirini Arvaniti, Kim Fricker, Michael Moret, Niels Rupp, Thomas Hermanns, Christian Fankhauser, Norbert Wey, Peter Wild, Jan Hendrik Rüschoff, and Manfred Claassen. Replication Data for: Automated Gleason grading of prostate cancer tissue microarrays via deep learning., 2018. [3](#), [6](#)
- [4] Marc Aubreville, Nikolas Stathonikos, Taryn A Donovan, Robert Klopfeisch, Jonas Ammeling, Jonathan Ganz, Frauke Wilm, Mitko Veta, Samir Jabari, Markus Eckstein, et al. Domain generalization across tumor types, laboratories, and species—insights from the 2022 edition of the mitosis domain generalization challenge. *Medical Image Analysis*, 94:103155, 2024. [3](#), [6](#)
- [5] Jinze Bai, Shuai Bai, Shusheng Yang, Shijie Wang, Sinan Tan, Peng Wang, Junyang Lin, Chang Zhou, and Jingren Zhou. Qwen-vl: A versatile vision-language model for understanding, localization, text reading, and beyond. *arXiv preprint arXiv:2308.12966*, 2023. [5](#)
- [6] Andrew A Borkowski, Marilyn M Bui, L Brannon Thomas, Catherine P Wilson, Lauren A DeLand, and Stephen M Mastorides. Lung and colon cancer histopathological image dataset (lc25000). *arXiv preprint arXiv:1912.12142*, 2019. [5](#)
- [7] Mathilde Caron, Hugo Touvron, Ishan Misra, Hervé Jégou, Julien Mairal, Piotr Bojanowski, and Armand Joulin. Emerging properties in self-supervised vision transformers. In *Proceedings of the IEEE/CVF international conference on computer vision*, pages 9650–9660, 2021. [2](#)
- [8] Pingyi Chen, Honglin Li, Chenglu Zhu, Sunyi Zheng, Zhongyi Shui, and Lin Yang. Wscaption: Multiple instance generation of pathology reports for gigapixel whole-slide images. In *International Conference on Medical Image Computing and Computer-Assisted Intervention*, pages 546–556. Springer, 2024. [1](#), [2](#), [3](#)
- [9] Pingyi Chen, Chenglu Zhu, Sunyi Zheng, Honglin Li, and Lin Yang. Wsi-vqa: Interpreting whole slide images by generative visual question answering. In *European Conference on Computer Vision*, pages 401–417. Springer, 2025. [2](#), [3](#)
- [10] Richard J Chen, Chengkuan Chen, Yicong Li, Tiffany Y Chen, Andrew D Trister, Rahul G Krishnan, and Faisal Mahmood. Scaling vision transformers to gigapixel images via hierarchical self-supervised learning. In *Proceedings of the IEEE/CVF Conference on Computer Vision and Pattern Recognition*, pages 16144–16155, 2022. [1](#)
- [11] Richard J Chen, Tong Ding, Ming Y Lu, Drew FK Williamson, Guillaume Jaume, Andrew H Song, Bowen Chen, Andrew Zhang, Daniel Shao, Muhammad Shaban, et al. Towards a general-purpose foundation model for computational pathology. *Nature Medicine*, 30(3):850–862, 2024. [1](#), [2](#)
- [12] Wenliang Dai, Junnan Li, Dongxu Li, Anthony Meng Huat Tiong, Junqi Zhao, Weisheng Wang, Boyang Li, Pascale N Fung, and Steven Hoi. Instructblip: Towards general-purpose vision-language models with instruction tuning. *Advances in Neural Information Processing Systems*, 36, 2024. [5](#)
- [13] Jevgenij Gamper and Nasir Rajpoot. Multiple instance captioning: Learning representations from histopathology textbooks and articles. In *Proceedings of the IEEE/CVF conference on computer vision and pattern recognition*, pages 16549–16559, 2021. [3](#)
- [14] Zhengrui Guo, Jiabo Ma, Yingxue Xu, Yihui Wang, Liansheng Wang, and Hao Chen. Histgen: Histopathology report generation via local-global feature encoding and cross-modal context interaction. *arXiv preprint arXiv:2403.05396*, 2024. [1](#), [2](#), [3](#)
- [15] Chu Han, Xipeng Pan, Lixu Yan, Huan Lin, Bingbing Li, Su Yao, Shanshan Lv, Zhenwei Shi, Jinhai Mai, Jiatai Lin, et al. Wss4lud: Grand challenge on weakly-supervised tissue semantic segmentation for lung adenocarcinoma. *arXiv preprint arXiv:2204.06455*, 2022. [5](#)
- [16] Zhi Huang, Federico Bianchi, Mert Yuksekogul, Thomas J Montine, and James Zou. A visual-language foundation model for pathology image analysis using medical twitter. *Nature medicine*, 29(9):2307–2316, 2023. [2](#), [3](#), [5](#)
- [17] Binyuan Hui, Jian Yang, Zeyu Cui, Jiayi Yang, Dayiheng Liu, Lei Zhang, Tianyu Liu, Jiajun Zhang, Bowen Yu, Kai Dang, et al. Qwen2. 5-coder technical report. *arXiv preprint arXiv:2409.12186*, 2024. [2](#)
- [18] Xinmi Huo, Kok Haur Ong, Kah Weng Lau, Laurent Gole, David M Young, Char Loo Tan, Xiaohui Zhu, Chongchong Zhang, Yonghui Zhang, Longjie Li, et al. A comprehensive ai model development framework for consistent gleason grading. *Communications Medicine*, 4(1):84, 2024. [6](#)
- [19] Wisdom Ikezogwo, Saygin Seyfioglu, Fatemeh Ghezloo, Dylan Geva, Fatwir Sheikh Mohammed, Pavan Kumar Anand, Ranjay Krishna, and Linda Shapiro. Quilt-1m: One million image-text pairs for histopathology. *Advances in Neural Information Processing Systems*, 36, 2024. [2](#), [3](#)
- [20] Wisdom Oluchi Ikezogwo, Mehmet Saygin Seyfioglu, Fatemeh Ghezloo, Dylan Stefan Chan Geva, Fatwir Sheikh Mohammed, Pavan Kumar Anand, Ranjay Krishna, and Linda Shapiro. Quilt-1m: One million image-text pairs for histopathology, 2023. [5](#)
- [21] Gabriel Ilharco, Mitchell Wortsman, Ross Wightman, Cade Gordon, Nicholas Carlini, Rohan Taori, Achal Dave,

- Vaishaal Shankar, Hongseok Namkoong, John Miller, Hananeh Hajishirzi, Ali Farhadi, and Ludwig Schmidt. Openclip, 2021. If you use this software, please cite it as below. 4
- [22] Maximilian Ilse, Jakub M Tomczak, and Max Welling. Attention-based deep multiple instance learning. *arXiv preprint arXiv:1802.04712*, 2018. 7
- [23] Dongsheng Jiang, Yuchen Liu, Songlin Liu, Jin’e Zhao, Hao Zhang, Zhen Gao, Xiaopeng Zhang, Jin Li, and Hongkai Xiong. From clip to dino: Visual encoders shout in multi-modal large language models. *arXiv preprint arXiv:2310.08825*, 2023. 2
- [24] Mingu Kang, Heon Song, Seonwook Park, Donggeun Yoo, and Sérgio Pereira. Benchmarking self-supervised learning on diverse pathology datasets. In *Proceedings of the IEEE/CVF Conference on Computer Vision and Pattern Recognition*, pages 3344–3354, 2023. 2
- [25] Jakob Nikolas Kather, Niels Halama, and Alexander Marx. 100,000 histological images of human colorectal cancer and healthy tissue. *Zenodo10*, 5281, 2018. 4, 6
- [26] Yoo Jung Kim, Hyungjoon Jang, Kyoungbun Lee, Seongkeun Park, Sung-Gyu Min, Choyeon Hong, Jeong Hwan Park, Kanggeun Lee, Jisoo Kim, Wonjae Hong, et al. Paip 2019: Liver cancer segmentation challenge. *Medical image analysis*, 67:101854, 2021. 6
- [27] Katharina Kriegsmann, Frithjof Lobers, Christiane Zgorzelski, Joerg Kriegsmann, Charlotte Janssen, Rolf Ruedinger Meliss, Thomas Muley, Ulrich Sack, Georg Steinbuss, and Mark Kriegsmann. Deep learning for the detection of anatomical tissue structures and neoplasms of the skin on scanned histopathological tissue sections. *Frontiers in Oncology*, 12:1022967, 2022. 5
- [28] Vinay Kumar, Abul K Abbas, Nelson Fausto, and Jon C Aster. *Robbins and Cotran pathologic basis of disease, professional edition e-book*. Elsevier health sciences, 2014. 1
- [29] Bin Li, Yin Li, and Kevin W Eliceiri. Dual-stream multiple instance learning network for whole slide image classification with self-supervised contrastive learning. In *Proceedings of the IEEE/CVF Conference on Computer Vision and Pattern Recognition*, pages 14318–14328, 2021. 7
- [30] Haotian Liu, Chunyuan Li, Yuheng Li, and Yong Jae Lee. Improved baselines with visual instruction tuning, 2023. 5
- [31] Haotian Liu, Chunyuan Li, Yuheng Li, Bo Li, Yuanhan Zhang, Sheng Shen, and Yong Jae Lee. Llava-next: Improved reasoning, ocr, and world knowledge, 2024. 4
- [32] Ming Y Lu, Bowen Chen, Drew FK Williamson, Richard J Chen, Ivy Liang, Tong Ding, Guillaume Jaume, Igor Odintsov, Long Phi Le, Georg Gerber, et al. A visual-language foundation model for computational pathology. *Nature Medicine*, 30(3):863–874, 2024. 1, 2
- [33] Ming Y Lu, Bowen Chen, Drew FK Williamson, Richard J Chen, Melissa Zhao, Aaron K Chow, Kenji Ikemura, Ahronng Kim, Dimitra Pouli, Ankush Patel, et al. A multimodal generative ai copilot for human pathology. *Nature*, pages 1–3, 2024. 1, 2
- [34] OpenAI. Gpt-4 technical report, 2023. 2
- [35] OpenAI. Gpt-4v(ision) system card. https://cdn.openai.com/papers/GPTV_System_Card.pdf, 2023. 2, 5
- [36] Maxime Oquab, Timothée Darcet, Théo Moutakanni, Huy Vo, Marc Szafraniec, Vasil Khalidov, Pierre Fernandez, Daniel Haziza, Francisco Massa, Alaaeldin El-Nouby, et al. Dinov2: Learning robust visual features without supervision. *arXiv preprint arXiv:2304.07193*, 2023. 1, 2
- [37] Alec Radford, Jong Wook Kim, Chris Hallacy, Aditya Ramesh, Gabriel Goh, Sandhini Agarwal, Girish Sastry, Amanda Askell, Pamela Mishkin, Jack Clark, Gretchen Krueger, and Ilya Sutskever. Learning transferable visual models from natural language supervision, 2021. 5
- [38] Alec Radford, Jong Wook Kim, Chris Hallacy, Aditya Ramesh, Gabriel Goh, Sandhini Agarwal, Girish Sastry, Amanda Askell, Pamela Mishkin, Jack Clark, et al. Learning transferable visual models from natural language supervision. In *International conference on machine learning*, pages 8748–8763. PMLR, 2021. 1, 2
- [39] Jeongun Ryu, Aaron Valero Puche, JaeWoong Shin, Seonwook Park, Biagio Brattoli, Jinhee Lee, Wonkyung Jung, Soo Ick Cho, Kyunghyun Paeng, Chan-Young Ock, Donggeun Yoo, and Sérgio Pereira. Ocelot: Overlapped cell on tissue dataset for histopathology. In *Proceedings of the IEEE/CVF Conference on Computer Vision and Pattern Recognition (CVPR)*, pages 23902–23912, 2023. 3, 6
- [40] Mehmet Saygin Seyfioglu, Wisdom O Ikezogwo, Fatemeh Ghezloo, Ranjay Krishna, and Linda Shapiro. Quilt-llava: Visual instruction tuning by extracting localized narratives from open-source histopathology videos. *arXiv preprint arXiv:2312.04746*, 2023. 2, 3
- [41] Mehmet Saygin Seyfioglu, Wisdom O Ikezogwo, Fatemeh Ghezloo, Ranjay Krishna, and Linda Shapiro. Quilt-llava: Visual instruction tuning by extracting localized narratives from open-source histopathology videos. In *Proceedings of the IEEE/CVF Conference on Computer Vision and Pattern Recognition*, pages 13183–13192, 2024. 1
- [42] George Shaikovski, Adam Casson, Kristen Severson, Eric Zimmermann, Yi Kan Wang, Jeremy D Kunz, Juan A Retamero, Gerard Oakley, David Klimstra, Christopher Kanan, et al. Prism: A multi-modal generative foundation model for slide-level histopathology. *arXiv preprint arXiv:2405.10254*, 2024. 3
- [43] Julio Silva-Rodríguez, Adrián Colomer, María A Sales, Rafael Molina, and Valery Naranjo. Going deeper through the gleason scoring scale: An automatic end-to-end system for histology prostate grading and cribriform pattern detection. *Computer methods and programs in biomedicine*, 195: 105637, 2020. 5
- [44] Julio Silva-Rodríguez, Adrián Colomer, María A. Sales, Rafael Molina, and Valery Naranjo. Going deeper through the gleason scoring scale: An automatic end-to-end system for histology prostate grading and cribriform pattern detection. *Computer Methods and Programs in Biomedicine*, 195: 105637, 2020. 6
- [45] Dario Sitnik, Gorana Aralica, Mirko Hadžija, Marijana Popović Hadžija, Arijana Pačić, Marija Milković Periša,

- Luka Manojlović, Karolina Krstanac, Andrija Plavetić, and Ivica Kopriva. A dataset and a methodology for intraoperative computer-aided diagnosis of a metastatic colon cancer in a liver. *Biomedical Signal Processing and Control*, 66: 102402, 2021. 3, 6
- [46] Yuxuan Sun, Yunlong Zhang, Yixuan Si, Chenglu Zhu, Zhongyi Shui, Kai Zhang, Jingxiong Li, Xingheng Lyu, Tao Lin, and Lin Yang. Pathgen-1.6 m: 1.6 million pathology image-text pairs generation through multi-agent collaboration. *arXiv preprint arXiv:2407.00203*, 2024. 1, 2, 3, 5
- [47] Yuxuan Sun, Chenglu Zhu, Sunyi Zheng, Kai Zhang, Lin Sun, Zhongyi Shui, Yunlong Zhang, Honglin Li, and Lin Yang. Pathasst: A generative foundation ai assistant towards artificial general intelligence of pathology. In *Proceedings of the AAAI Conference on Artificial Intelligence*, pages 5034–5042, 2024. 1, 2, 3, 5
- [48] Gemini Team, Rohan Anil, Sebastian Borgeaud, Yonghui Wu, Jean-Baptiste Alayrac, Jiahui Yu, Radu Soricut, Johan Schalkwyk, Andrew M Dai, Anja Hauth, et al. Gemini: a family of highly capable multimodal models. *arXiv preprint arXiv:2312.11805*, 2023. 2, 5
- [49] Yuri Tolkach, Lisa Marie Wolgast, Alexander Damanakis, Alexey Pryalukhin, Simon Schallenberg, Wolfgang Hulla, Marie-Lisa Eich, Wolfgang Schroeder, Anirban Mukhopadhyay, Moritz Fuchs, et al. Artificial intelligence for tumour tissue detection and histological regression grading in oesophageal adenocarcinomas: a retrospective algorithm development and validation study. *The Lancet Digital Health*, 5(5):e265–e275, 2023. 3, 6
- [50] Bastiaan S Veeling, Jasper Linmans, Jim Winkens, Taco Cohen, and Max Welling. Rotation equivariant cnns for digital pathology. In *Medical Image Computing and Computer Assisted Intervention—MICCAI 2018: 21st International Conference, Granada, Spain, September 16–20, 2018, Proceedings, Part II 11*, pages 210–218. Springer, 2018. 4
- [51] Eugene Vorontsov, Alican Bozkurt, Adam Casson, George Shaikovski, Michal Zelechowski, Siqi Liu, Kristen Severson, Eric Zimmermann, James Hall, Neil Tenenholtz, et al. Virchow: A million-slide digital pathology foundation model. *arXiv preprint arXiv:2309.07778*, 2023. 2
- [52] Jerry Wei, Arief Suriawinata, Bing Ren, Xiaoying Liu, Mikhail Lisovsky, Louis Vaickus, Charles Brown, Michael Baker, Naofumi Tomita, Lorenzo Torresani, et al. A petri dish for histopathology image analysis. In *Artificial Intelligence in Medicine: 19th International Conference on Artificial Intelligence in Medicine, AIME 2021, Virtual Event, June 15–18, 2021, Proceedings*, pages 11–24. Springer, 2021. 6
- [53] F. Wilm, M. Fragoso, C. Marzahl, C. Bertram, R. Klopffleisch, A. Maier, M. Aubreville, and K. Breininger. Canine cutaneous cancer histology dataset, 2022. 3, 6
- [54] Feng Xu, Chuang Zhu, Wenqi Tang, Ying Wang, Yu Zhang, Jie Li, Hongchuan Jiang, Zhongyue Shi, Jun Liu, and Mulan Jin. Predicting axillary lymph node metastasis in early breast cancer using deep learning on primary tumor biopsy slides. *Frontiers in Oncology*, page 4133, 2021. 3, 6
- [55] Gang Xu, Zhigang Song, Zhuo Sun, Calvin Ku, Zhe Yang, Cancheng Liu, Shuhao Wang, Jianpeng Ma, and Wei Xu. Camel: A weakly supervised learning framework for histopathology image segmentation. In *2019 IEEE/CVF International Conference on Computer Vision (ICCV)*, pages 10681–10690, 2019. 3, 6
- [56] Hanwen Xu, Naoto Usuyama, Jaspreet Bagga, Sheng Zhang, Rajesh Rao, Tristan Naumann, Cliff Wong, Zelalem Gero, Javier González, Yu Gu, et al. A whole-slide foundation model for digital pathology from real-world data. *Nature*, pages 1–8, 2024. 1, 2
- [57] An Yang, Baosong Yang, Binyuan Hui, Bo Zheng, Bowen Yu, Chang Zhou, Chengpeng Li, Chengyuan Li, Dayiheng Liu, Fei Huang, et al. Qwen2 technical report. *arXiv preprint arXiv:2407.10671*, 2024. 2
- [58] Jiahui Yu, Zirui Wang, Vijay Vasudevan, Legg Yeung, Mojtaba Seyedhosseini, and Yonghui Wu. Coca: Contrastive captioners are image-text foundation models. *arXiv preprint arXiv:2205.01917*, 2022. 3, 4
- [59] Ying Zeng and Jialong Zhu. Transferring the knowledge of vision-language model for pathological image classification. In *2024 IEEE 2nd International Conference on Sensors, Electronics and Computer Engineering (ICSECE)*, pages 94–98, 2024. 6
- [60] Sheng Zhang, Yanbo Xu, Naoto Usuyama, Hanwen Xu, Jaspreet Bagga, Robert Tinn, Sam Preston, Rajesh Rao, Mu Wei, Naveen Valluri, et al. Biomedclip: a multimodal biomedical foundation model pretrained from fifteen million scientific image-text pairs. *arXiv preprint arXiv:2303.00915*, 2023. 5
- [61] Eric Zimmermann, Eugene Vorontsov, Julian Viret, Adam Casson, Michal Zelechowski, George Shaikovski, Neil Tenenholtz, James Hall, Thomas Fuchs, Nicolo Fusi, et al. Virchow 2: Scaling self-supervised mixed magnification models in pathology. *arXiv preprint arXiv:2408.00738*, 2024. 1, 2
- [62] Barret Zoph, Vijay Vasudevan, Jonathon Shlens, and Quoc V. Le. Learning transferable architectures for scalable image recognition, 2018. 3, 6

CPath-Omni: A Unified Multimodal Foundation Model for Patch and Whole Slide Image Analysis in Computational Pathology

Supplementary Material

A. Additional Experiments and Details

A.1. Ablations of Vision and Text Components in CPath-CLIP

We further explore the influence of different vision and text components on CPath-CLIP’s performance in zero-shot tasks to explore its semantic alignment capabilities and understand the role of each element. Our experiments include evaluating CLIP-L alone, Virchow2 alone, and a combination of both, as well as fixing the vision encoder and comparing text encoders by substituting CLIP-L with Qwen2-1.5B. As shown in Tab. B.1, when using Virchow2 as the fixed vision backbone and replacing the CLIP-L text encoder with Qwen2-1.5B, we observe a 0.9% overall performance improvement. Conversely, fixing the text encoder as Qwen2-1.5B and replacing CLIP-L with Virchow2 results in a significant 13.7% performance increase. This suggests that the primary boost is attributed to Virchow2’s pathology-specific pretraining on 3.1 million whole-slide images, highlighting that a more advanced pathology encoder greatly enhances semantic alignment capabilities. Furthermore, combining CLIP-L with Virchow2 provides an additional 0.3% performance boost. While this gain is modest compared to the standalone Virchow2 encoder, we retain it to enrich semantic features for future integration into LLM.

A.2. CPath-Omni Performance in Patch and WSI Classification Tasks

Tab. B.2, Tab. B.3, and Tab. B.4 present detailed metrics for patch-level and WSI-level classification corresponding to the radar plot visualization shown in Fig. 4 of the main paper. We also compare state-of-the-art pathology LMMs, Quilt-LLaVA, and PathGen-LLaVA. Notably, these models cannot directly perform WSI classification. To adapt them for this task, we employ the same method used with GPT-4o in the main paper: generating captions for individual patches and merging them into a WSI-level report, which is then used for classification based on predefined questions. Further details are available in Section 5.5 of the main paper.

Our findings show that CPath-Omni significantly outperforms previous models in both patch-level and WSI-level classification tasks. Notably, in out-of-distribution or zero-shot patch classification datasets (Tab. B.3), none of the models were trained on these datasets, making it a relatively fairer comparison. In this context, CPath-Omni signifi-

cantly surpasses GPT-4o and Gemini-1.5-Pro, the strongest general models, as well as pathology-specific LMMs such as PathGen-LLaVA and Quilt-LLaVA. Additionally, CPath-Omni achieves performance comparable to task-specific fine-tuned models, underscoring its strength in task unification and exceptional overall performance.

A.3. Experiment Details of Patch-level Linear Probing and Task-Specific Model Fine-Tuning

Linear Probing: The linear probing experiment evaluates the representational power of a pre-trained model by adding a linear layer to its output. This linear layer maps the model’s output vector to the number of classes, enabling classification. The experiment uses a batch size of 32 and runs for 20 epochs. The optimizer is AdamW with a learning rate of 1×10^{-2} . To ensure robustness and reproducibility, we employ 10 different seeds. The procedure involves randomly selecting N samples (2, 8, 16, 32, 64, 128) from each class to form the training set. If an official test set is unavailable or lacks labels, the remainder of the dataset serves as the test set. Throughout the 20 epochs, we select the best-performing model based on its accuracy on the test set, providing insights into the effectiveness of the added linear layer in classifying unseen data.

Task-specific model fine-tuning: For task-specific model fine-tuning, we build on the linear probing setup by unfreezing the Virchow2 backbone and performing full-parameter fine-tuning on the model using the entire training set.

A.4. Details for WSI preprocessing

For WSI preprocessing, we utilize CLAM to identify and segment regions by setting appropriate thresholds. Within each WSI, we extract 2048×2048 non-overlapping patches at a magnification of $40\times$ from the identified regions. Patches are retained if more than 10% of their area contains valid tissue regions. Additionally, each 2048×2048 patch is further subdivided into one 2048×2048 patch, four 1024×1024 patches, and sixteen 512×512 patches for subsequent feature extraction.

A.5. Details for WSI Task-Specific Fine-Tuning

The models are trained for 20 epochs without a learning rate schedule, using a fixed learning rate of 1×10^{-5} . The training process utilizes the Adam optimizer without weight decay, and the batch size is consistently set to 1.

Model Architecture. The MIL framework commonly used for WSI classification includes three learnable components:

(1) A fully-connected layer to reduce the dimensionality of features to 256. (2) An attention network to aggregate and transform the instance features. (3) A final fully-connected layer for making predictions. We experiment with ABMIL and DSMIL. Both models share the same fully connected layers for reducing feature dimensionality and making predictions. For the attention network, ABMIL uses the gated attention mechanism, while DSMIL introduces a dual-stream architecture.

For a fair comparison, the input patch features of these two models are kept consistent with those of CPath-Omni.

A.6. Training Hyperparameters for CPath-CLIP and CPath-Omni

We detail the training parameters of CPath-CLIP in Tab. B.6. The hyperparameters for the four training stages of CPath-Omni are listed in Tab. B.7, Tab. B.8, Tab. B.9, and Tab. B.10, respectively. Specifically, stages 1 and 2 focus on patch-based training, stage 3 is dedicated to WSI-based training, and stage 4 involves a mix of patch-based and WSI-based training.

A.7. Hardware

We employ 8 NVIDIA H800-80G GPUs to train the CPath-Omni model, 1 NVIDIA A100-40G GPU for fine-tuning task-specific models, and 4 NVIDIA H800-80G GPUs for caption generation using PathGen-LLaVA and Quilt-LLaVA.

B. Additional Details of Collected Datasets

We provide details on the dataset sources and distribution of CPath-PatchCaption in Fig. B.1. The sources, quantities, distributions, and sub-task data allocations for CPath-PatchInstruction and CPath-WSIInstruction are also illustrated in Fig. B.2 and Fig. B.3.

Additionally, the construction of CPath-VQA within the CPath-Instruct dataset follows a systematic approach. First, we collect datasets that already include captions. For datasets lacking captions, such as classification datasets, we use GPT-4o to generate captions by combining classification labels with image data. GPT-4o further generates VQA pairs from these captioning datasets, creating the CPath-VQA.

We also present visualization examples of the novel task of visual referring prompting, alongside tasks specific to whole-slide images, which differ from natural images due to their extremely high resolution, reaching nearly $100,000 \times 100,000$ pixels. Specifically, Fig. B.4 illustrates the annotation interface for visual referring prompting and shows how pathologists annotate this task. Fig. B.5 provides an example of generating visual referring prompting. Fig. B.6 showcases examples of WSI captioning and VQA. In these

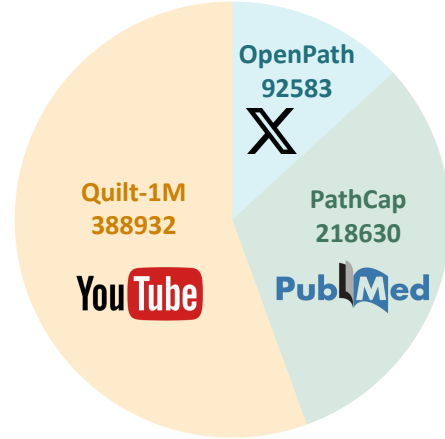


Figure B.1. CProportions of sub-datasets in CPath-PatchCaption and their primary sources.

examples, we present the cleaned report, which, after processing, aligns well with the pathological representations in the whole-slide image. We highlight the correspondences between features in the report and the whole-slide image for better clarity. Based on this cleaned report, we generate both multiple-choice and open-ended examples.

C. Prompts for GPT-4o

This section presents all the prompts used in our dataset and experimental process, including: (1) the prompt in Figure Fig. C.7, which is used with GPT-4o to enrich and refine existing image captions by adding details; (2) the prompt in Figure Fig. C.8, which is utilized to modify raw WSI reports by removing information that cannot be directly observed in the WSI, such as gross specimen descriptions; (3) the prompts in Fig. C.9 and Fig. C.10, which are applied to generate closed-ended and open-ended VQA pairs based on cleaned WSI reports; (4) the prompt in Fig. C.11, which is designed to prompt GPT-4o to generate captions for image patches within a WSI; (5) the prompt in Fig. C.12, which is used to merge all the captions generated for individual patches in a WSI into a cohesive generated WSI report; (6) the prompts in Fig. C.13 and Fig. C.14, which are employed to guide GPT-4o in answering closed-ended and open-ended WSI VQAs by analyzing whether the answers can be derived from the generated WSI report; and (7) the prompt in Figure C.15, which is used to determine whether the answer to an open-ended WSI VQA is correct by referencing the provided question and answer.

Vision Encoder		Text Encoder	LC-Lung	LC-Colon	CRC100K	SkinCancer	Pcam	BACH	Osteo	WSSSLUAD	SICAPv2	Average
CLIP-L	Virchow2											
✗	✓	CLIP-L	94.9	99.5	77.7	70.1	91.1	74.5	72.7	89.9	67.9	82.0
✗	✓	Qwen2-1.5B	96.8	99.8	76.0	78.1	94.6	72.0	82.0	86.4	60.7	82.9
✓	✗	Qwen2-1.5B	92.1	91.9	67.0	61.7	87.8	47.5	52.9	79.0	42.9	69.2
✓	✓	Qwen2-1.5B	97.1	100.0	78.0	74.2	95.9	72.3	80.7	87.1	63.1	83.2

Table B.1. Zero-shot classification performance comparison of CPath-CLIP built with different vision and text encoders.

	GPT-4o	Gemini-1.5-pro	Quilt-LLaVA	PathGen-LLaVA	Full-finetune	CPath-Omni (ours)
VALSET_TCGA	39.2	28.0	23.5	28.9	97.0	<u>96.0</u>
Stomach	18.7	33.3	21.6	19.6	83.2	<u>82.6</u>
KIRC	79.8	84.4	38.2	90.8	<u>99.4</u>	99.6
CocaHis	90.0	60.0	43.4	89.7	88.0	90.0
PAIP23	30.0	47.8	14.5	15.9	89.4	<u>88.4</u>
VALSET_WNS	29.5	26.2	17.3	23.3	93.8	<u>91.2</u>
BCNB	52.0	65.8	65.7	65.2	90.4	<u>90.0</u>
VALSET_CHA	30.2	30.6	16.2	25.2	96.6	<u>93.2</u>
CATCH	20.4	36.0	26.7	26.7	<u>79.0</u>	83.2
PAIP21	7.0	37.4	18.9	18.1	92.6	<u>86.2</u>
MIDOG22	47.7	62.1	50.9	48.9	<u>65.8</u>	80.2
KICH	74.0	73.0	29.6	87.1	<u>99.4</u>	100.0
CAMEL	64.2	53.4	56.7	61.0	<u>91.4</u>	92.4
Gleason_CNN	46.3	51.8	38.8	39.0	81.7	81.7
OCELOT	44.2	27.3	20.9	37.2	90.9	<u>84.4</u>
NASNetLarge	62.8	54.4	50.4	54.5	<u>97.6</u>	99.0
Average	46.0	48.2	33.3	45.7	<u>89.8</u>	89.9

Table B.2. Performance comparison of general-purpose, pathology-specific, and task-specific models on ID patch classification tasks.

	GPT-4o	Gemini-1.5-pro	Quilt-LLaVA	PathGen-LLaVA	CPath-Omni (ours)
SkinCancer	33.7	30.2	6.7	42.4	89.4
LC25000-Lung	46.7	57.5	63.2	<u>79.8</u>	92.1
LC25000-Colon	81.3	87.5	92.1	100.0	100.0
CRC100K	59.8	39.9	16.2	57.1	<u>57.4</u>
BACH	29.7	36.3	15.3	<u>42.1</u>	88.8
WSSSLUAD	<u>62.5</u>	60.0	42.1	43.9	85.1
PatchCamylon17	<u>64.4</u>	34.6	58.1	66.2	52.7
Osteo	<u>63.3</u>	54.2	33.6	34.9	78.9
MHIST	<u>50.0</u>	53.8	<u>50.0</u>	<u>50.0</u>	47.4
SICAPv2	<u>41.3</u>	35.6	25.7	26.9	80.9
AGGC2022	<u>51.3</u>	36.8	18.1	27.4	84.4
KIRP	74.6	77.7	59.7	<u>92.2</u>	99.2
PAIP19	54.4	<u>71.8</u>	33.4	43.1	89.4
VALSET_UKK	<u>39.4</u>	30.4	23.1	19.1	87.6
Average	<u>53.7</u>	50.5	38.4	51.8	81.0

Table B.3. Performance comparison of general-purpose and pathology-specific models on OOD patch classification tasks.

	ABMIL	DSMIL	GPT-4o	PRISM	Quilt-LLaVA	PathGen-LLaVA	CPath-Omni (ours)
TCGA-THCA	<u>58.7</u>	59.9	37.6	32.3	29.5	40.5	58.5
TCGA-RCC	95.7	<u>95.3</u>	43.0	50.3	38.6	51.1	94.0
TCGA-ESCA	97.4	97.4	73.7	79.0	63.2	76.3	92.1
TCGA-NSCLC	91.1	87.2	58.8	81.1	58.8	65.5	<u>88.8</u>
TCGA-UCEC	93.4	83.0	42.9	41.4	47.0	47.4	<u>87.8</u>
TCGA-BLCA	60.3	61.7	54.1	<u>68.8</u>	51.4	53.7	70.7
TCGA-BRCA	82.4	<u>86.7</u>	50.6	83.5	48.1	60.5	89.2
TCGA-TGCT	<u>72.6</u>	<u>72.1</u>	42.9	27.4	20.5	39.3	80.9
Average	<u>81.5</u>	80.4	50.5	58.0	44.6	54.3	82.8

Table B.4. Performance comparison of general-purpose and pathology-specific models on WSI classification tasks using balanced accuracy.

Dataset	Classes
PatchCamelyon	<i>'lymph node', 'lymph node metastasis'</i>
NCK-CRC	<i>'Adipose', 'Debris', 'Lymphocytes', 'Mucus', 'Smooth muscle', 'Normal colon mucosa', 'Cancer-associated stroma', 'Colorectal adenocarcinoma epithelium'</i>
LC25000Lung	<i>'Lung adenocarcinoma', 'benign lung tissue', 'lung squamous cell carcinomas'</i>
LC25000Colon	<i>'Colon adenocarcinoma', 'normal colon tissue'</i>
BACH	<i>'Benign tissue', 'In-situ carcinoma', 'Invasive carcinoma', 'Normal tissue'</i>
SICAPv2	<i>'Non-cancerous', 'Atrophic well differentiated and dense glandular regions', 'Cribriform, ill-formed, large-fused and papillary glandular patterns', 'Isolated cells or file of cells, nests of cells without lumina formation and pseudo-rosetting patterns'</i>
Osteo	<i>'Non-tumor', 'Necrotic tumor', 'Viable tumor'</i>
SkinCancer	<i>'Non-tumor chondral tissue', 'Non-tumor dermis', 'Non-tumor elastosis', 'Non-tumor epidermis', 'Non-tumor hair follicle', 'Non-tumor skeletal muscle', 'Non-tumor necrosis', 'Non-tumor nerves', 'Non-tumor sebaceous glands', 'Non-tumor subcutis', 'Non-tumor sweat glands', 'Non-tumor vessel', 'Tumor epithelial basal cell carcinoma', 'Tumor epithelial squamous cell carcinoma', 'Tumor melanoma', 'Tumor naevus'</i>
WSSSLUAD	<i>'tumor', 'normal'</i>

Table B.5. Classes for each dataset in zero-shot image classification. Consistent prompt templates are used for all datasets, including: 'An H&E image of {}', 'This is an image of {} presented in the image', and 'An H&E patch of {}'.

Hyper-parameter	Value
Num GPUs	8
Num epochs	5
Learning rate	3e-5
Per device train batch size	64
Gradient accumulation steps	1
Weight decay	0.1
Warmup steps	300

Table B.6. Hyperparameters used in CPath-CLIP training.

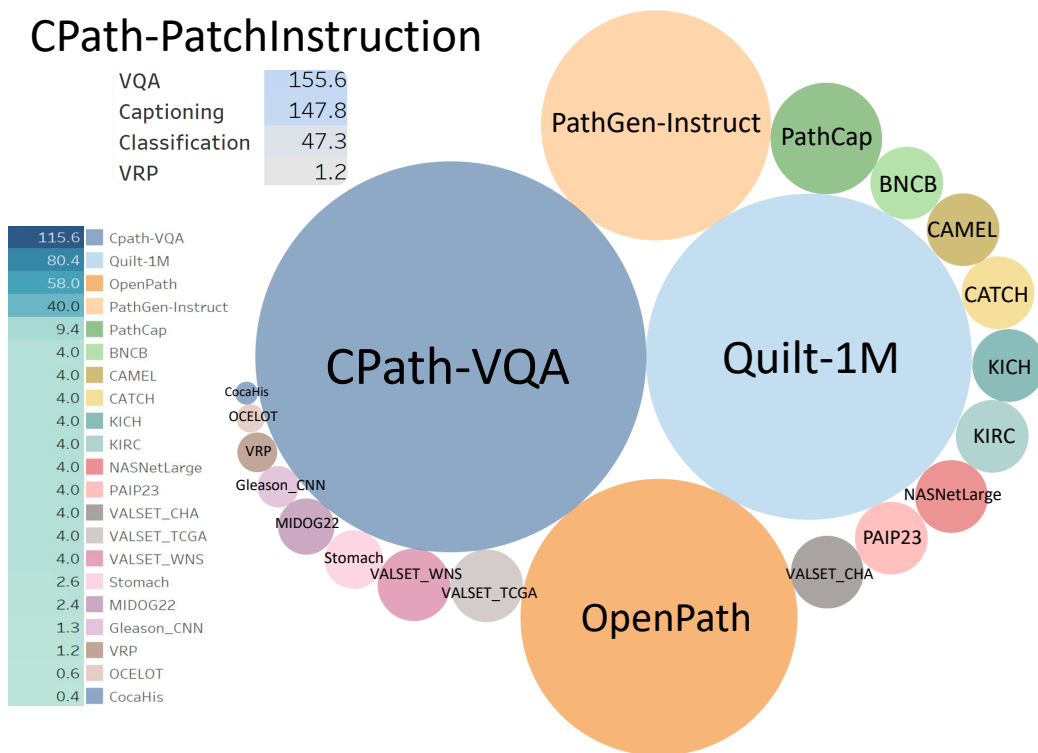


Figure B.2. Visualization of the datasets used in CPath-PatchInstruct, including their quantities (in thousands) and proportional distributions, where larger circles represent higher proportions.

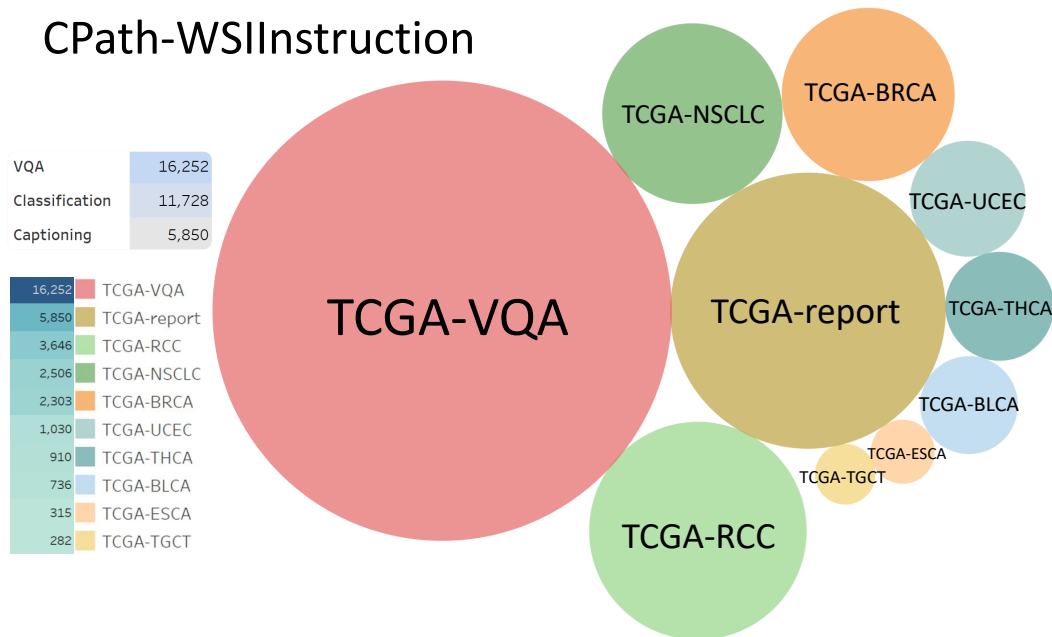


Figure B.3. Visualization of the datasets used in CPath-WSIInstruct, including their quantities and proportional distributions, where larger circles represent higher proportions.

morphology

The image shows clusters of cells with a glandular or acinar arrangement, which is typical for pancreatic tissue. 1

The cells within these clusters have moderately abundant cytoplasm and round to oval nuclei. Some nuclei appear slightly enlarged and hyperchromatic. 2

There is a noticeable desmoplastic reaction in the surrounding stroma, characterized by dense fibrous tissue. 3

The stroma also contains scattered inflammatory cells, including lymphocytes and possibly plasma cells. 4

The nuclei within the cell clusters show mild pleomorphism, with some variation in size and shape. 5

There is no significant atypia or prominent nucleoli observed. 6

Mitotic figures are not prominently visible in this section. 7

There are duct-like structures present, some of which appear dilated. 8

The lining epithelium of these ducts does not show significant atypia but may exhibit mild reactive changes. 9

No clear evidence of necrosis or hemorrhage is noted in this section. 0

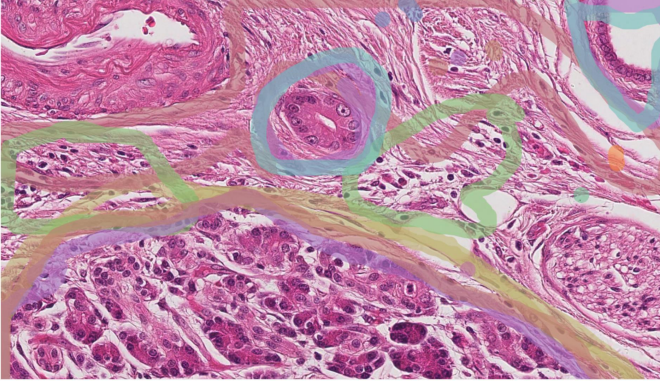
The overall architecture suggests a disruption of normal pancreatic acinar structure. q

diagnosis

The presence of desmoplastic stroma, mild nuclear pleomorphism, and disrupted acinar architecture are suggestive of pancreatic adenocarcinoma. w

The desmoplastic reaction and architectural distortion are key features supporting the diagnosis of pancreatic adenocarcinoma. o

A definitive diagnosis would require correlation with clinical findings, additional histological sections, and possibly immunohistochemical staining. t



Info History

Selection Details

The stroma also contains scattered inflammatory cells, including lymphocytes and possibly plasma cells. ID 4TePbn8U-a

The nuclei within the cell clusters show mild pleomorphism, with some variation in size and shape.

The nuclei in the cell clusters are not found to be abnormal.

There is no significant atypia or prominent nucleoli observed.

Mitotic figures are not prominently visible in this section.

Regions Relations

Manual By Time

Update

morphology

The histology image of the endometrium shows a dense fibrous stroma with scattered glandular structures. 1

The glands are irregularly shaped and lined by columnar epithelial cells. 2

Some of the epithelial cells exhibit nuclear atypia. 3

There is a notable presence of stromal fibrosis, characterized by thick bundles of collagen fibers interspersed with spindle-shaped stromal cells. 4

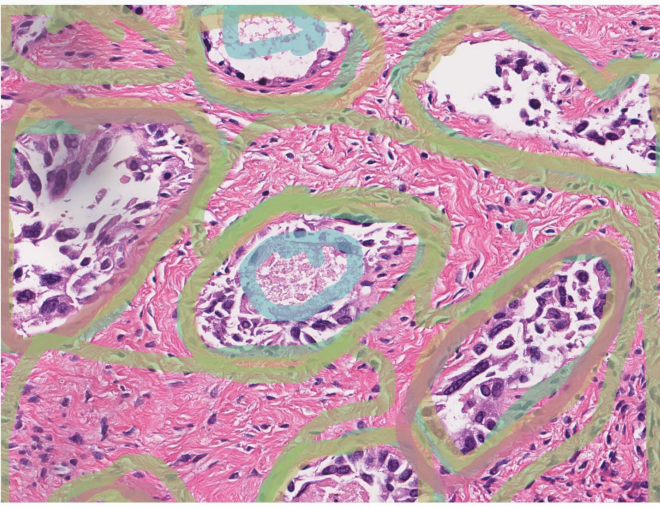
The glandular lumina contain eosinophilic secretions. 5

The overall architecture suggests a disorganized pattern. 6

diagnosis

The features may be indicative of a pathological process such as endometrial hyperplasia or a neoplastic condition. 7

Further clinical correlation and additional diagnostic tests would be necessary for a definitive diagnosis. 8



Info History

Selection Details

Some of the epithelial cells exhibit nuclear atypia.

There is a notable presence of stromal fibrosis, characterized by thick bundles of collagen fibers interspersed with spindle-shaped stromal cells.

The glandular lumina contain eosinophilic secretions.

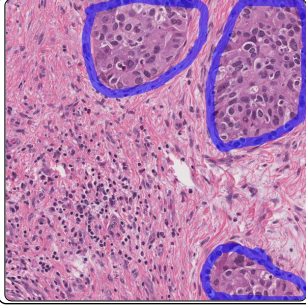
The overall architecture suggests a disorganized pattern.

Regions Relations

Manual By Time

Update

Figure B.4. Examples of the pathologist annotation interface for visual referring prompting. Pathologists are required to verify whether the given morphology and diagnosis are correct, record "T" or "F" in the bottom-right corner, or modify the original findings as needed. Once all findings are confirmed accurate, they use corresponding colored markers to highlight the regions in the image associated with each finding.

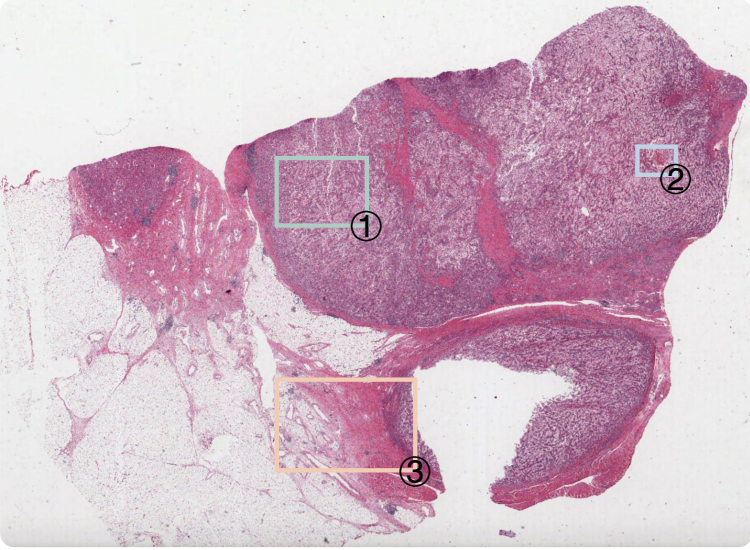


Visual referring prompting (VRP)

Question: What can be observed in the circled areas of this liver histology slide regarding the structural organization of the cells?

Answer: In the circled areas, the liver architecture is disrupted by malignant cells arranged in nests and sheets. These cells exhibit significant pleomorphism, and prominent nucleoli, displaying an irregular arrangement indicative of invasive carcinoma, which is consistent with hepatocellular carcinoma (HCC).

Figure B.5. An example of a constructed visual referring prompting task, where questions are answered based on the highlighted regions.



Cleaned Report

Microscopic examination of the right kidney nephrectomy specimen reveals a renal cell carcinoma of the conventional (clear cell) type. The neoplastic cells exhibit Fuhrman grade 4 nuclear features with prominent nucleoli. The architecture includes areas of sarcomatoid dedifferentiation. Focal necrosis is present within the tumor. Invasion into adjacent adipose tissue is noted, alongside evidence of angiolymphatic invasion, characterized by a tumor thrombus within a nearby vessel. The non-neoplastic kidney tissue does not show any specific abnormalities.

VQA (Multi-choice)

Question: What is the Fuhrman nuclear grade of the neoplastic cells in the image?

(A) Grade 2 (B) Grade 3
(C) Grade 1 (D) Grade 4

VQA (Open-ended)

Question: Where is the invasion of perinephric adipose tissue observed?

Answer: Invasion is noted in the perinephric adipose tissue on the lateral aspect of the kidney.

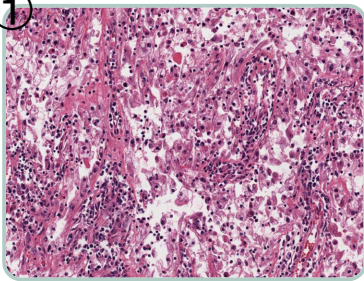
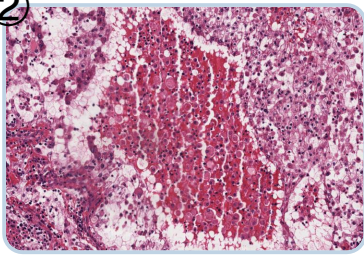
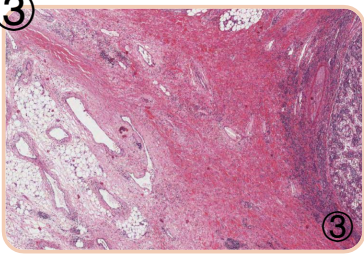
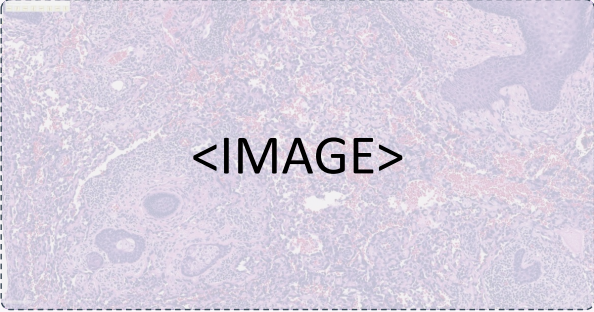




Figure B.6. Examples of WSI Captioning and VQA tasks, where corresponding findings in the captions are highlighted with matching colored boxes in the WSI.



Please conduct a detailed analysis of the microscopic image featuring cells or tissues or overall structure with the logic of a professional pathologist, and provide an expert-level pathology image description. Focus on identifying the morphological characteristics of the cells and tissues or providing a diagnosis based solely on direct observations from the image. Follow these guidelines:

1. Visible Features Only: Describe only those features that are visible and identifiable in the image. Concentrate solely on the characteristics or diagnosis of the displayed cells or tissues or overall structure.
2. Accuracy (most important!!): Ensure that your response is entirely based on the image and fully accurate. Avoid including any descriptions that are uncertain.
3. Locate the described features: If possible, specify the exact position of the described features within the image, including the relative location to other pathology objects. You can describe the image in order of positions or include the location after each observation.
4. Avoid Speculation: Do not speculate about details that are not visible in the image, such as elements that would require higher magnification or other staining.
5. Only provide a diagnosis if you are very certain: Offer a diagnosis only if you are highly confident, explaining the rationale behind your conclusion. If certainty is not possible, refrain from making a diagnosis.
6. Direct Output: Present your final description directly as you are directly observing the image. In one paragraph.

Additional description: {description}



Figure C.7. Prompt for GPT-4o to generate a detailed description for an image based on its original caption.

Please revise this slide report by eliminating any details that cannot be directly observed under the H&E microscope image (e.g., area, thickness, tumor dimensions, or other information not visible through staining). Focus exclusively on the microscopic characteristics and diagnostic features seen in the H&E whole slide image. Present your observations concisely as a professional pathologist analyzing the slide in one clear paragraph.

Report: {report}



Figure C.8. Prompt for GPT-4o to clean the raw data from the WSI report, transforming it into accurate ground truth WSI report.

Please generate 5-10 clinically meaningful quantitative or qualitative multiple-choice questions based on the single whole-slide image report mentioned above. The questions should require visual examination of whole-slide microscopic images to be answered. Do not include words or content directly from the report and do not provide hints in the questions. Please format your response in JSON, for example: [{"question": "xxx", "options": [option1, option2, ...], "answer": "xxx"}, ...]

Report: {report}



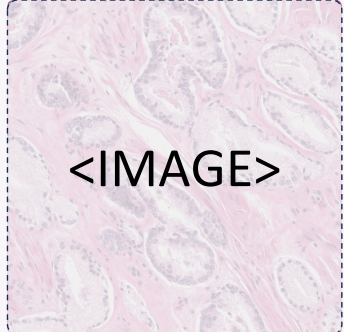
Figure C.9. Prompt for GPT-4o to generate closed-ended VQA based on a given WSI report.

Please generate 5-10 clinically meaningful quantitative or qualitative multi-choice question-and-answer pairs based on the single whole-slide image report mentioned above. The questions should require visual examination of whole-slide microscopic images to be answered. Avoid questions that can be answered solely with medical knowledge without needing to examine the microscopic pathology images. If the content from the report is insufficient, generate fewer questions accordingly. Do not include words or content directly from the report or provide too many hints in the questions. Please format your response in JSON, for example:
[{"question": "xxx", "answer": "xxx"}, ...]

Report: {report}



Figure C.10. Prompt for GPT-4o to generate open-ended VQA based on a given WSI report.



Please conduct a thorough examination of this microscopic image featuring cells or tissues and provide an expert-level pathology image description. Identify the morphological characteristics of the cells and tissues, or provide a diagnosis based solely on what you directly observe. Only output critical findings in 1-2 sentence.



Figure C.11. Prompt for GPT-4o to generate the caption for WSI patch image.

Summarize the following patch captions to generate a concise report for the entire whole slide image, presented in one coherent paragraph.

Patch captions: {captions}



Figure C.12. Prompt for GPT-4o to merge generated patch captions into a comprehensive WSI report.

According to the given pathology whole slide image report, answer the question. Only output the option index.

Report: {report}



Figure C.13. Prompt for GPT-4o to answer the closed-ended question based on the generated WSI report.

According to the given pathology whole slide image report, answer the question in short.

Report: {report}



Figure C.14. Prompt for GPT-4o to answer the open-ended question based on the generated WSI report.

Please determine whether the prediction is correct based on the question and the reference answer. Provide your response, outputting only 'yes' or 'no.'

Question: {question}

Predicted: {predicted answer}

Reference: {reference answer}



Figure C.15. Prompt for GPT-4o to determine whether the predicted answer to the open-ended question is correct.

Hyper-parameter	Value
LLM Model	Qwen2.5-14B-Instruct
Vision Model	CPath-CLIP
Tunable parts	MLP
Vision select layer	-2
Model max length	8192
Image aspect ratio	Square
Image grid pinpoints	None
Patch merge type	Flat
Prompt version	Plain
Num GPUs	8
Num epochs	1
Learning rate	1e-3
Per device train batch size	16
Gradient accum steps	1
Weight decay	0.
Warmup ratio	0.03
Lr scheduler type	cosine

Table B.7. Hyperparameters used in stage 2 training of CPath-Omni (Patch pretraining).

Hyper-parameter	Value
LLM Model	Qwen2.5-14B-Instruct
Vision Model	CPath-CLIP
Tunable parts	CPath-CLIP & MLP & LLM
Vision select layer	-2
Model max length	32768
Image aspect ratio	AnyRes (up to 9 splits)
Image grid pinpoints	(1x1),..., (3x3)
Patch merge type	Spatial unpad
Prompt version	Qwen-1.5
Num GPUs	8
Num epochs	1
Learning rate	1e-5
Per device train batch size	1
Gradient accum steps	8
Weight decay	0.
Warmup ratio	0.03
Lr scheduler type	cosine
Vision tower lr	2e-6

Table B.8. Hyperparameters used in stage 2 training of CPath-Omni (Patch fine-tuning).

Hyper-parameter	Value
LLM Model	Qwen2.5-14B-Instruct
Vision Model	CPath-CLIP
Tunable parts	WSI projector
Vision select layer	-2
Model max length	8192
WSI hidden size	3328
Image aspect ratio	Square
Image grid pinpoints	None
Patch merge type	Flat
Prompt version	Plain
Num GPUs	8
Num epochs	1
Learning rate	5e-6
Per device train batch size	16
Gradient accum steps	1
Weight decay	0.
Warmup ratio	0.1
Lr scheduler type	cosine

Table B.9. Hyperparameters used in stage 3 training of CPath-Omni (WSI pretraining).

Hyper-parameter	Value
LLM Model	Qwen2.5-14B-Instruct
Vision Model	CPath-CLIP
Tunable parts	CPath-CLIP & MLP & WSI projector & LLM
Vision select layer	-2
Model max length	32768
Wsi hidden size	3328
Image aspect ratio	AnyRes (up to 9 splits)
Image grid pinpoints	(1x1),..., (3x3)
Patch merge type	Spatial unpad
Prompt version	Qwen-1.5
Num GPUs	8
Num epochs	5
learning rate	1e-5
Per device train batch size	1
Gradient accum steps	8
Weight decay	0.
Warmup ratio	0.1
Lr scheduler type	cosine
WSI projector lr	1e-5
Vision tower lr	2e-6

Table B.10. Hyperparameters used in stage 4 training of CPath-Omni (mixed patch and WSI fine-tuning).

Dataset	Source Link
TCGA	https://portal.gdc.cancer.gov/
CocaHis	https://portal.gdc.cancer.gov/
BCNB	https://bcnb.grand-challenge.org/
CAMELYON17	https://camelyon17.grand-challenge.org/Data/
MIDOG2022	https://midog.deepmicroscopy.org/download-dataset/
AGGC2022	https://aggc22.grand-challenge.org/
ARCH	https://warwick.ac.uk/fac/cross_fac/tia/data/arch
BACH	https://zenodo.org/records/3632035
CAMEL	https://drive.google.com/open?id=1brr8CnU6ddzAYT157wkdXjbSzoIIDF9y
LC2500	https://academictorrents.com/details/7a638ed187a6180fd6e464b3666a6ea0499af4af
MIDOG2021	https://imig.science/midog2021/download-dataset/
OCELOT	https://zenodo.org/record/7844149
Osteo	https://www.cancerimagingarchive.net/collection/osteosarcoma-tumor-assessment/
PAIP2019	https://paip2019.grand-challenge.org/
PAIP2020	https://paip2020.grand-challenge.org/
PAIP2021	https://paip2021.grand-challenge.org/
SICAPv2	https://data.mendeley.com/datasets/9xxm58dvs3/1
CRC-100K	https://zenodo.org/records/1214456
PCam	https://github.com/basveeling/pcam
HistGen	https://github.com/dddavid4real/HistGen
PathGen-Instruct	https://github.com/PathGen-1-6M/PathGen-1.6M
PathCap	https://huggingface.co/datasets/jamessyx/PathCap
OpenPath	https://drive.google.com/drive/folders/1b5UT8BzUphkHZavRG-fmiyY9JWYIWZER
Quilt-1M	https://github.com/wisdomikezogwo/quilt1m
PathMMU	https://huggingface.co/datasets/jamessyx/PathMMU
CocaHis	https://www.sciencedirect.com/science/article/abs/pii/S1746809420305085?via%3Dihub
OCELOT	https://ocelot2023.grand-challenge.org/datasets
Gleason_CNN	https://github.com/eiriniar/gleason_CNN
MIDOG22	https://midog2022.grand-challenge.org
VALSET	https://zenodo.org/records/7548828
PAIP23	https://2023paip.grand-challenge.org/
NASNetLarge	https://zenodo.org/records/3825933
RCdpia (KIRC, KICH, KIRP)	http://39.171.241.18:8888/RCdpia/annotation.php
CATCH	https://www.cancerimagingarchive.net/collection/catch/
SkinCancer	https://heidata.uni-heidelberg.de/dataset.xhtml?persistentId=doi:10.11588/data/7QCR8S
MHIST	https://bmirids.github.io/MHIST
WSSSLUAD	https://wsss4luad.grand-challenge.org/
LC25000	https://github.com/tampapath/lung_colon_image_set?tab=readme-ov-file

Table B.11. Datasets used in this study with corresponding access links